

Source-generated noise on multicomponent records

Susan L.M. Miller, Malcolm B. Bertram and Don C. Lawton

ABSTRACT

An examination of shot records from a multicomponent seismic reflection survey showed that the converted-wave bandwidth overlapped with the surface-wave bandwidth. Rayleigh-wave energy was 2 to 3 times higher on the radial channel than on the vertical channel. The single-point receiver vertical records displayed more surface-wave noise than equivalent records obtained using conventional geophones in arrays. After bandpass filtering, noise levels on both records were comparable. Far-offset multicomponent records showed less surface-wave contamination than near-offset shots, but reflection signal was masked by multiple-refraction energy on both components. Geophones were effective at separating components so that reflection signal was retained even when there was higher amplitude noise in the orthogonal direction. P-P and P-SV reflection amplitudes were approximately equivalent at outer offsets but could not be measured at near offsets due to noise contamination. At near offsets, the A/D resolution of the recording instruments was insufficient to recover converted-wave signal from beneath high-amplitude surface-wave and headwave energy.

INTRODUCTION

Source-generated noise frequently has high amplitudes which can overwhelm or seriously degrade signal. In reflection seismic surveys, noise refers to any coherent or incoherent energy other than reflection signal of the desired polarization. Two types of high-amplitude, coherent noise which commonly appear on shot records are surface-wave and headwave energy.

Surface waves recorded by vertical and radial component geophones are Rayleigh waves. These move along the surface of a homogeneous half-space with retrograde elliptical particle motion in the vertical plane of the direction of propagation (Sheriff, 1984). The Rayleigh wave is usually high amplitude, low frequency (less than 12 Hz), and travels at about 0.9 times the shear-wave velocity in a Poisson solid. In a layered medium with varying shear-wave velocities, surface-wave energy is dispersive; i.e., different frequency components travel at different velocities. The amplitude of surface waves decreases exponentially with depth. Surface-wave energy may involve modes other than the pure Rayleigh wave and is often referred to by the more general term of ground roll.

Conventional seismic acquisition techniques have primarily employed two methods to reduce such noise. Because the frequency content of the P-wave signal and the surface-wave energy are quite well separated, low-cut filters can be applied in the field which will eliminate much of the low-frequency noise while still permitting most of the signal to pass. Additionally, geophones are generally laid out in arrays. If the array is in the order of one wavelength of the surface wave, the noise will be strongly attenuated, and even shorter arrays will help to reduce surface-wave amplitudes.

Neither of these methods is appropriate for multicomponent acquisition. Converted-wave energy may have lower frequency spectra than conventional data and in

fact may have a central frequency close to or within the noise spectrum. In this case, low-cut filtering attenuates signal as well as noise, and is ineffective as a means of separation. Logistics dictate that single-point receivers be used for acquiring multicomponent data. Each geophone requires careful planting, positioning and levelling if the data are to be reliable. The actual geophones are also larger and heavier than conventional geophones.

Without the use of low-cut filters and geophone arrays, Rayleigh waves and other low-frequency, source-generated noise can degrade the radial signal on multicomponent data. In fact, these conventional approaches should no longer be employed for the vertical component. Acquisition and processing parameters should be consistent for both components if the goal is to analyze the vector wave field.

Refraction energy is another form of coherent noise which can overwhelm reflection energy. On conventional data the first breaks can often be muted without damaging the signal. On the radial channel of multicomponent data, shallow converted reflections may appear before the shear-headwave so that a mute applied to the shear first breaks will also cut out shallow reflection signals. Due to emergence angle, P-headwave energy may leak onto the radial channel and obscure these shallow reflections.

It is important to determine how much noise attenuation can be done in the field without degrading signal quality. Conversely, if high-amplitude noise is recorded, how much signal can be recovered through processing? This information is necessary in order to design acquisition and processing parameters which will most effectively increase the signal-to-noise ratio (S/N).

The acquisition of multicomponent data allows us to study noise wave fields in three-dimensional space. For instance, Rayleigh-wave motion is completely described by the vertical and radial channels. Love waves, another type of surface wave, are detected on the transverse channel. A more complete characterization of noise is the first step in developing improved means of suppressing it. This has important applications for conventional seismic also, as improving the S/N ratio is one of the fundamental goals of seismic acquisition and processing techniques.

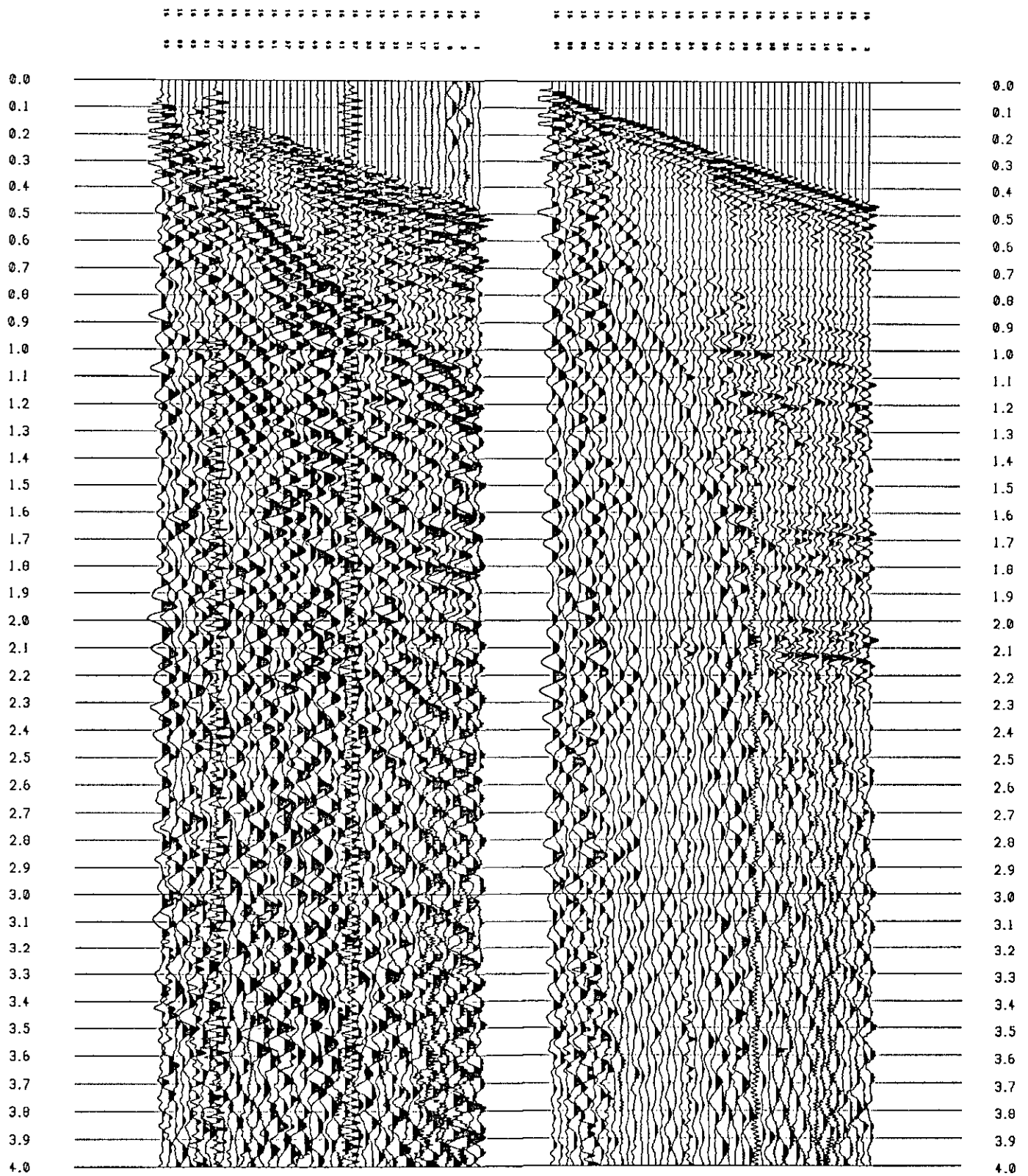
The purpose of this study was to characterize the bandwidth of both noise and signal on the vertical and radial components of several shot records. Absolute amplitudes of noise and signal were compared in order to assess the dynamic range required during recording for signal to be recovered during processing. Hodograms were used to examine the particle motion of certain events and thus determine the polarization of the received wave field.

The shot records examined here were acquired by the 1990 University of Calgary Geophysics Field School. The acquisition parameters for this survey are described by Lawton and Harrison (1990, this volume).

OBSERVATIONS

Figure 1 shows the radial and vertical shot records from shot 16, which had a near offset of 30 metres and was located near the western end of the line. The two components were recorded using single OYO geophones at a 30 metre spacing. The field low-cut filter was 20 Hz with a 12 dB/octave slope. An AGC scaling has been applied using a scaling window length of 700 ms. Traces are alternately numbered as the vertical and radial components were recorded on alternating channels.

A visual inspection of the records reveals some immediate differences between the two components. The signal-to-noise ratio is much poorer on the radial component. Almost the entire record is swamped with noise, making it difficult to discern any signal. The first arrival is the P-wave refraction. Just after this, at about 550 ms. on the far traces, is a P-SV reflection. It is significant that this event arrives before the S-headwave, which is the high-amplitude arrival at about 1150 ms. on the far traces.



1a. Radial channel of multicomponent data,
shot record 16.

1b. Vertical channel of multicomponent data,
shot record 16.

By contrast, the vertical record is noisy on the near half of the record, beyond which reflection energy is clearly visible. The overall frequency content of the vertical record is higher than that of the radial. Both records exhibit low-frequency, low-velocity, linear noise which appears to be ground roll. There is also considerable low-frequency, random noise, particularly on the near-offset traces.

The same record for the conventional line is displayed in Figure 2 for comparison. These are P-wave data which were recorded with a 12 Hz, 36 dB/octave low-cut filter and receiver arrays of nine conventional geophones spread over 30 metres, which was the group interval. There is less surface-wave energy on this record and reflections are visible across about 2/3 of the record. Comparing this to the vertical component of the multicomponent spread (Figure 2b) shows that the effect of the geophone array was to attenuate ground roll and other low-frequency shot noise. The two records were recorded with different low-cut filters, but the attenuation should be about the same for noise with a frequency of 10 to 12 Hz.

Figure 3 shows the radial and vertical components of shot 65, which had a near offset of 840 metres. The noise characteristics on both components are quite different to record 16. Both records from shot 65 show high-amplitude, multiple-refraction arrivals after the first breaks. These are reflected refractions which reverberate in a near-surface layer before arriving at surface. They represent a significant noise problem on these data as they have obscured much of the shallow reflection data. Reflected refractions are not as prominent on record 16, suggesting that there is a change in the near-surface character at the eastern end of the line.

Due to the increased offset, we do not observe significant ground roll on either component for record 65. On the vertical component the reflections can be followed across the entire record. However the radial component is again noisier, and signal energy is only coherent across about half the record. This is still an improvement over the near-offset record 16.

The other significant noise on record 65 is the high-frequency noise which dominates the lower half of both channels. This is wind noise which has been amplified by the gain. Because the bandwidth of this noise is not in the vicinity of the signal bandwidth, it can be eliminated by high-cut filtering.

ANALYSIS

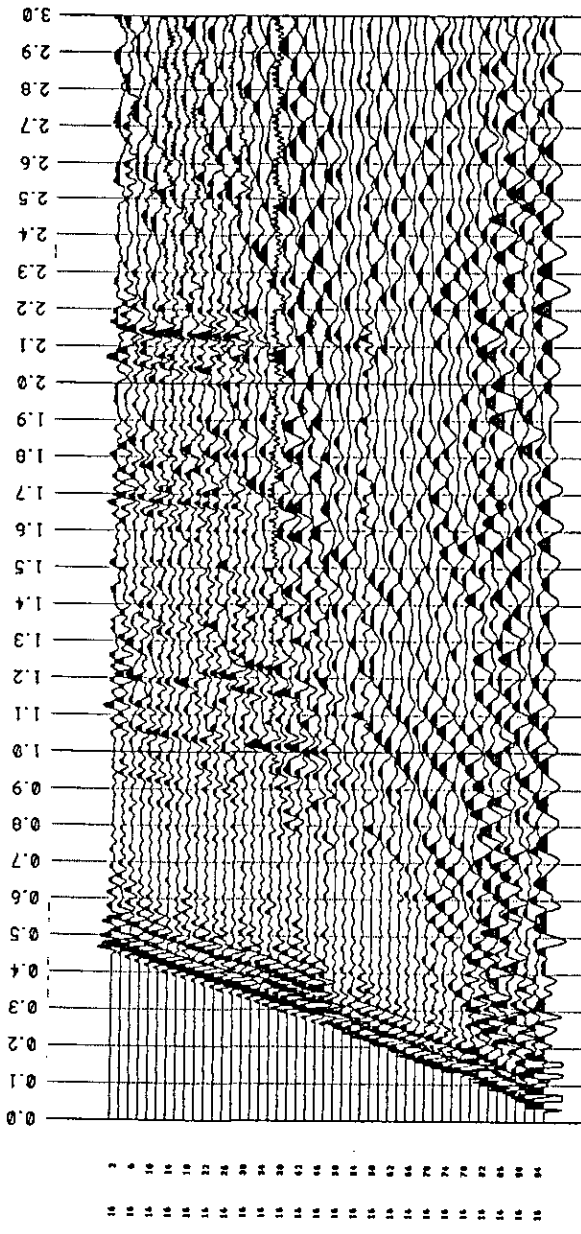
Frequency Bandwidth

In order to examine the implications of low-cut filtering in the field, we characterized the bandwidth of the various signal and noise events. Figure 4 shows the amplitude spectra for various signal and noise events on the vertical channel of record 16. All frequency analysis was done on raw, unscaled data. In each case the three adjacent traces shown have been windowed over the event of interest. Figure 4a is the amplitude spectra of traces 6, 7, and 8 windowed from 850 to 1250 ms. This window extends over a zone of reflection data in order to determine the frequency spectrum of the signal. The peak at 30 Hz is the dominant frequency of the reflection energy.

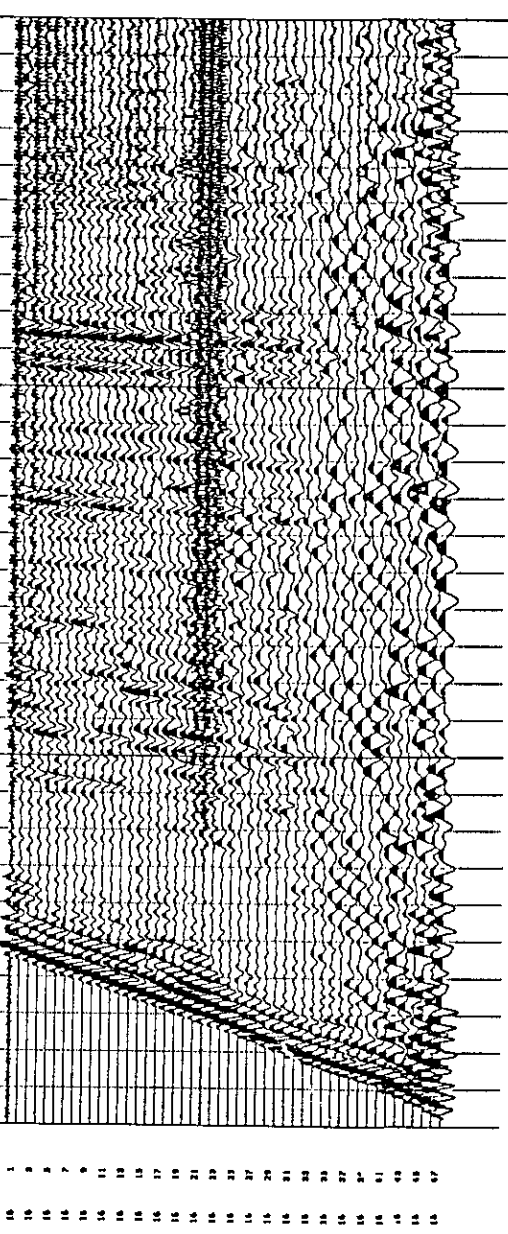
The separation of the reflection signal from the lower frequency noise indicates that a bandpass filter may be effective in recovering the signal from under the noise. In Figure 5 both the vertical channel of the multicomponent data and the conventional data have been filtered with a 15/20 - 60/80 bandpass. Although the conventional data has slightly better resolution in some regions, the records are generally comparable.

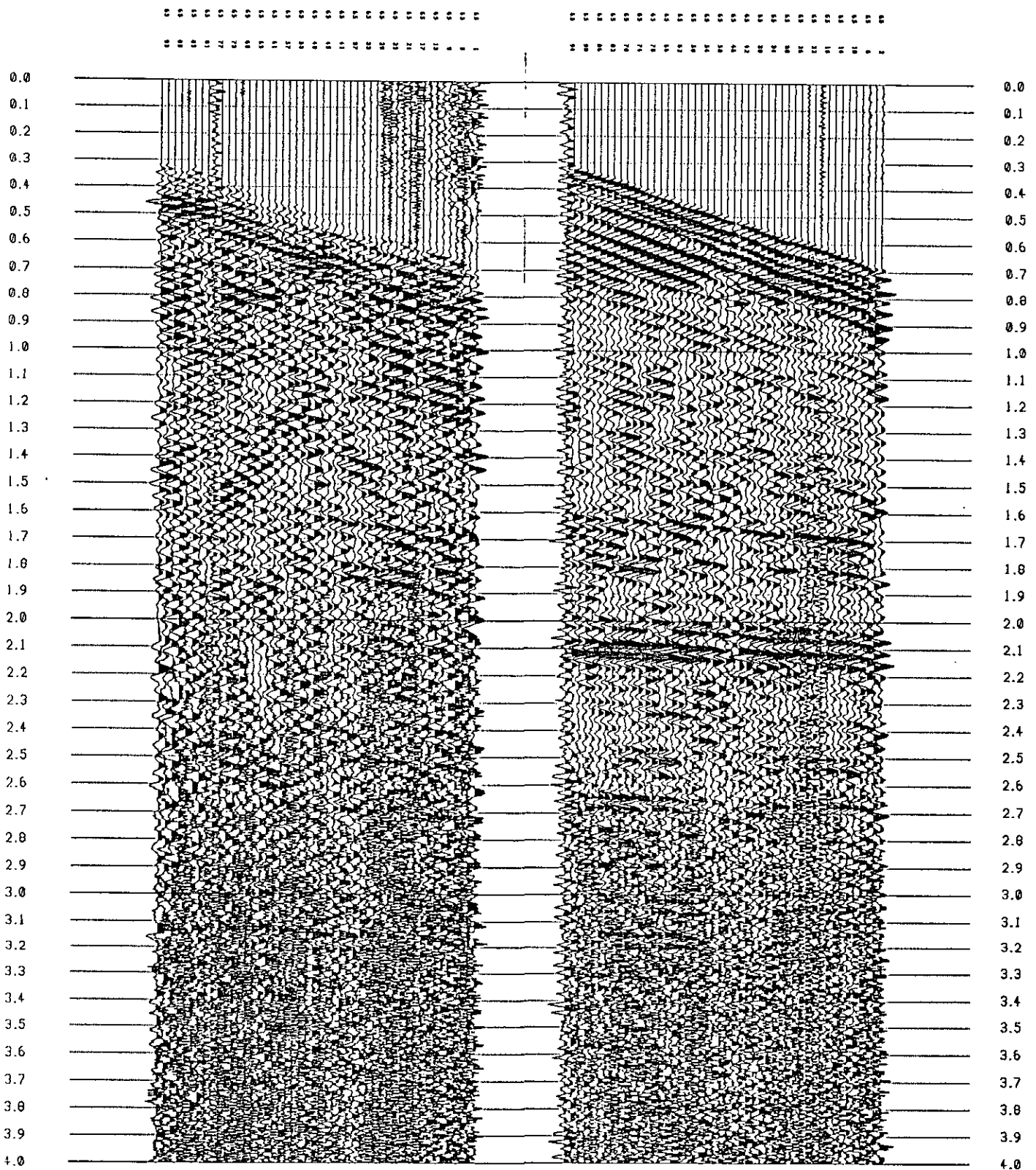
The other three spectra in Figure 4 represent different types of noise which were observed on the vertical record. Figure 4b is the spectrum for the P-wave refraction, taken

2b. Vertical channel of multicomponent data, shot record 16.



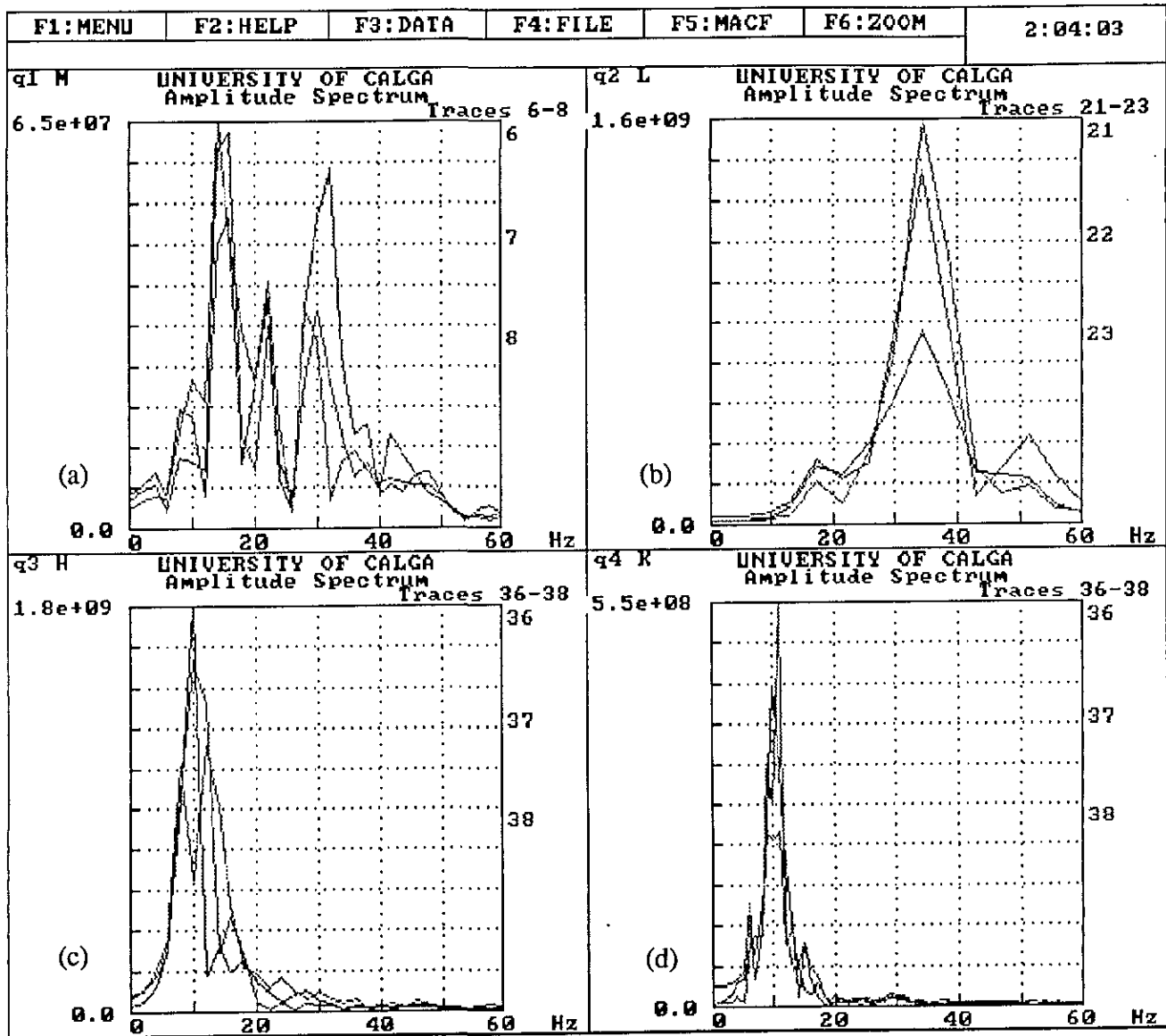
2a. Conventional data, shot record 16.



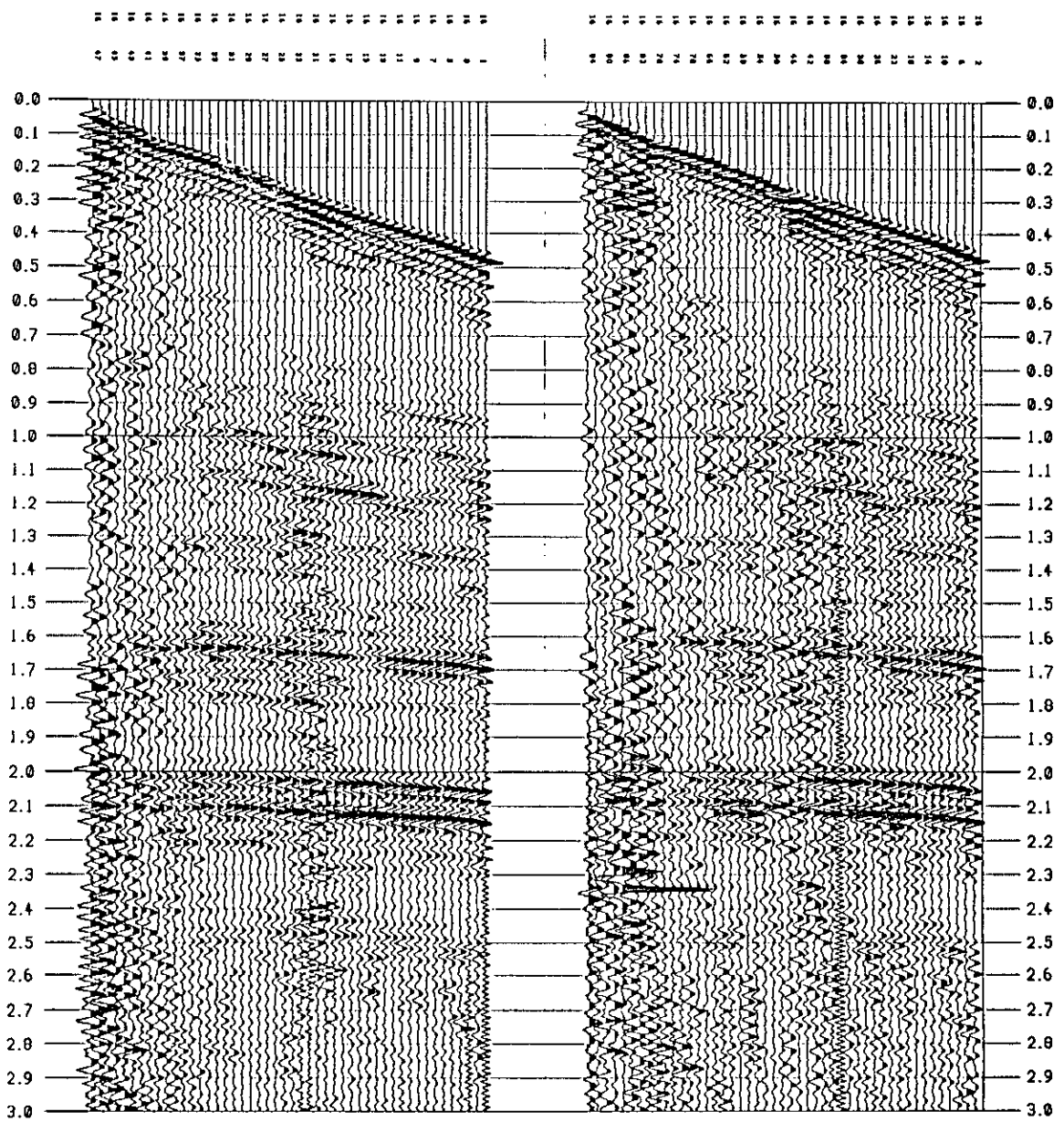


3a. Radial channel of multicomponent data, shot record 65.

3b. Vertical channel of multicomponent data, shot record 65.



4. Amplitude spectra from vertical channel, record 16: a) P-P reflection signal; b) P-headwave energy; c) surface-wave energy; d) random noise.



5a. Record from 2a, with 10/15 - 60/80 bandpass filter applied.

5b. Record from 2b, with 10/15 - 60/80 bandpass filter applied.

from traces 21 to 23 between 250 and 450 ms. The refraction energy has a peak frequency of 35 Hz, slightly higher than the reflection signal.

Figure 4c is the amplitude spectrum of the Rayleigh wave from traces 36 to 38, windowed from 800 to 1300 ms. The peak frequency is 10 Hz with a bandwidth from about 5 to 20 Hz. Figure 4d is derived from traces 36 to 38 also, but at a deeper time window, 2000 to 3000 ms. The noise in this zone appears to be completely random. It displays the same frequency character as the Rayleigh wave but is lower in amplitude.

Figure 6 displays the equivalent amplitude spectra for the radial component of record 16. Figure 6a shows spectra of reflection signals and are taken from the same geophones as the spectra for the P-wave signal. The window is also the same length, 1600 to 2000 ms., and extends over about the same interfaces. The dominant signal frequency of 15 Hz is an octave lower than the P-wave signal, and is overlapping with the ground roll bandwidth which peaks at 10 Hz.

The spectra in Figure 6b are from traces 36-38 windowed over the shear-wave refraction from 300 to 500 ms. The shear refraction has a dominant frequency of 32 Hz, comparable to the P-headwave and an octave higher than the SV-wave signal.

Figures 6c and 6d examine the same three traces at different times. The surface-wave energy arrives after the headwave, and, as indicated from the vertical record over the same time window, has a dominant frequency of 10 Hz. The coherency of the noise is lost later in the record. A window from 2000 to 3000 ms. has a bandwidth from 4 Hz to about 20 Hz. Again, the amplitude of the random noise is lower than the Rayleigh-wave amplitude.

Hodograms

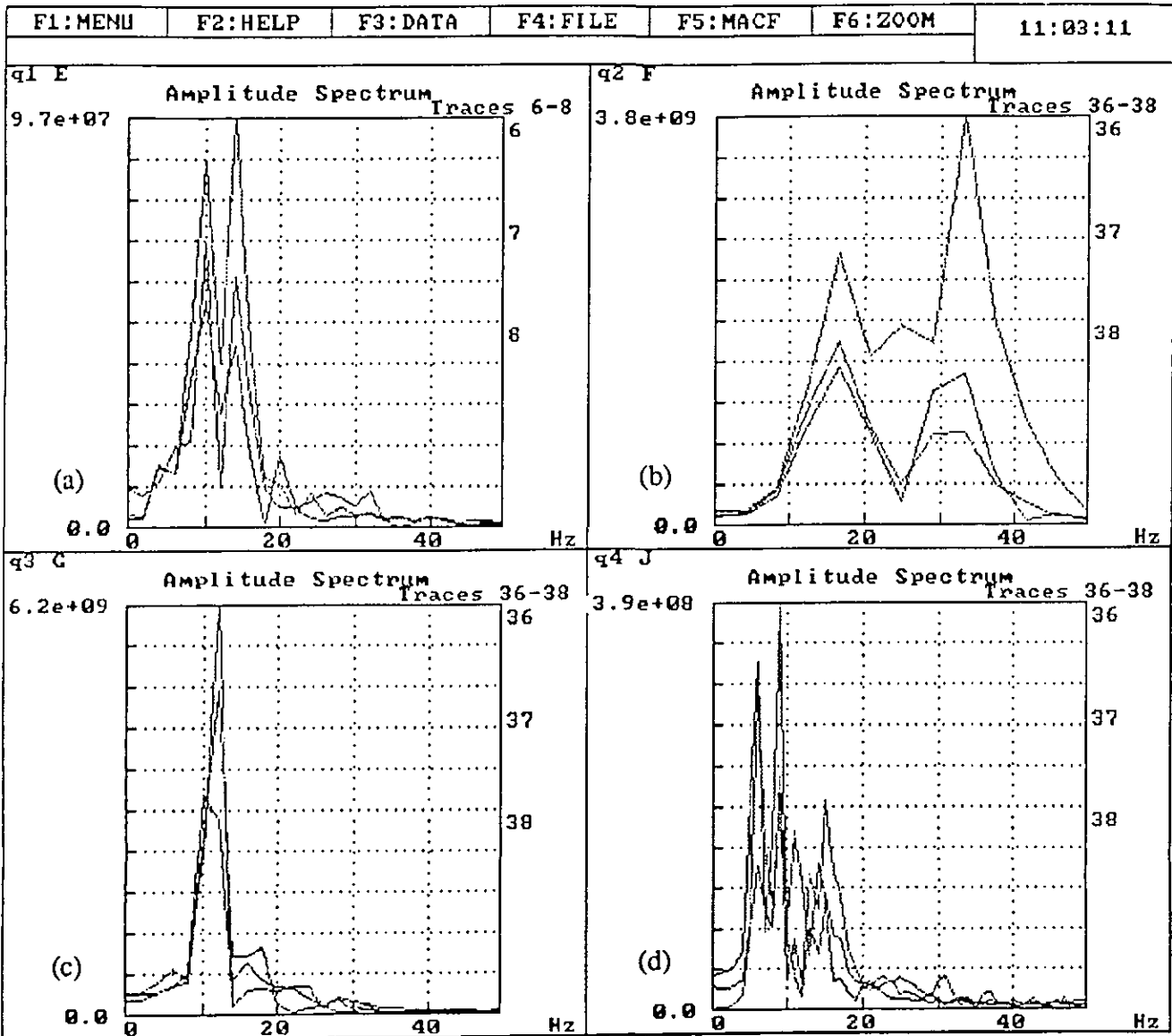
Hodograms were used to identify the polarization of events and to examine the dominant particle motion during a specific time window. The hodograms are scaled to the maximum excursion for each set of three. Thus the relative amplitudes within each figure (each set of three) are preserved but amplitudes between figures cannot be compared. (Trace numbers indicated on the figure are about double the actual trace number because radial and vertical components were recorded on alternate channels.)

Figure 7 are hodograms from traces 36 to 38 from 1000 to 1100 ms. The particle motion is elliptical and retrograde; that is, the particle motion at the top of the ellipse is in the opposite direction to the wave propagation. This identifies the linear noise observed on the shot records as Rayleigh waves. The major axis of the ellipse is on the radial axis, indicating that the amplitude of the Rayleigh wave is 2 to 3 times higher (ratio of major to minor axis) on the radial component than on the vertical component. The effect of the higher amplitude is seen in Figure 1, in which ground roll extends further across the record on the radial component than on the vertical component.

The particle motion of the incoherent, low-frequency noise observed on both components is shown in Figure 8. The chaotic shape of the hodograms and the lack of consistency from trace to trace indicate that these are complex wave fields. The amount of energy on the vertical and radial channels also varies between traces.

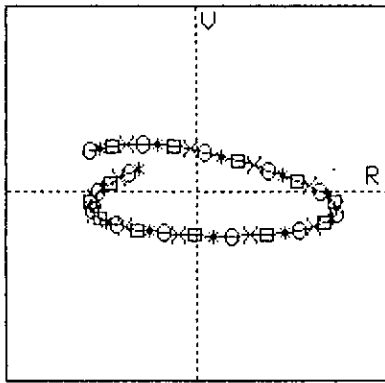
Hodograms were computed for the coherent energy at 1800 ms. on the radial component of record 16 to confirm its identity as a P-SV reflection. Figure 9 effectively demonstrates the radial polarization of the wave field. The hodogram also effectively demonstrates the variation in amplitude from trace to trace.

As pointed out earlier, there is a shallow P-SV reflection arriving shortly after the P-headwave and before the S-headwave on the radial component of record 16. Figure 10 shows the hodograms of three of the far-offset traces (4, 5, and 6 on the shot record). The dominant particle motion is actually vertical, indicating that the P-wave refractions are higher in amplitude than the shear-wave reflection. The vertical excursions are 2 to 3 times

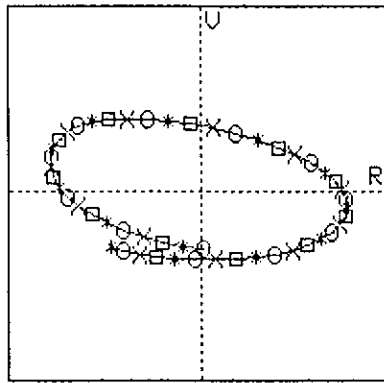


6. Amplitude spectra from radial channel, record 16: a) P-SV reflection signal; b) S-headwave energy; c) surface-wave energy; d) random noise.

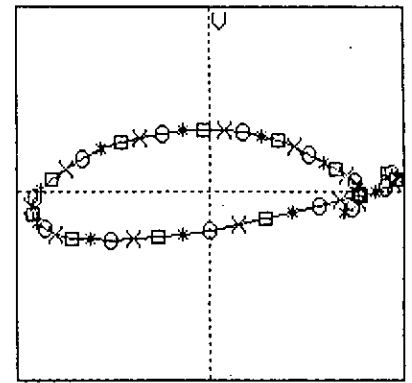
RECORD 16



Trace # (Radial) = 71
Trace # (Vertical) = 72
Start time [ms] = 1000
End time [ms] = 1100



Trace # (Radial) = 73
Trace # (Vertical) = 74
Start time [ms] = 1000
End time [ms] = 1100

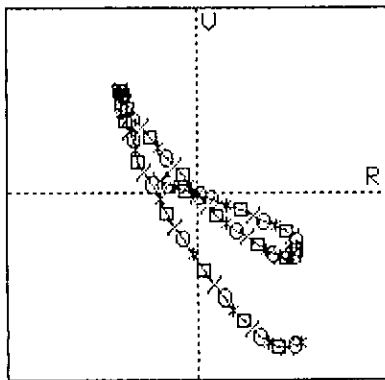


Trace # (Radial) = 75
Trace # (Vertical) = 76
Start time [ms] = 1000
End time [ms] = 1100

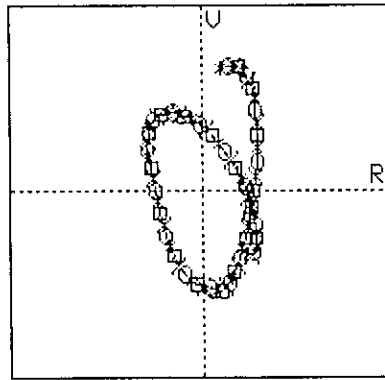
Sample interval [ms] = 2 * - O - X - □

7. Hodograms of Rayleigh waves.

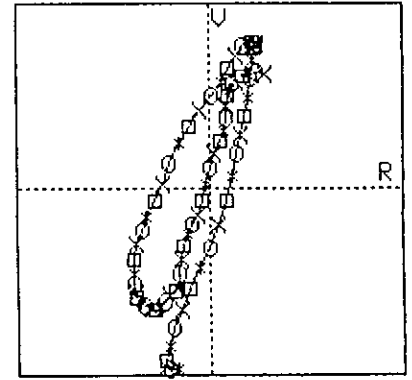
RECORD 16



Trace # (Radial) = 71
Trace # (Vertical) = 72
Start time [ms] = 2250
End time [ms] = 2400



Trace # (Radial) = 73
Trace # (Vertical) = 74
Start time [ms] = 2250
End time [ms] = 2400

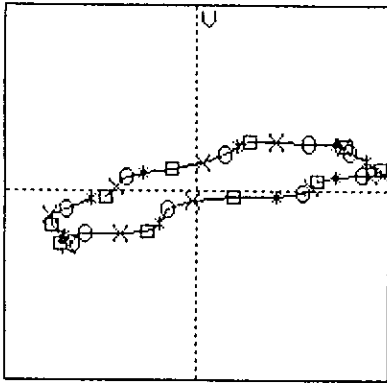


Trace # (Radial) = 75
Trace # (Vertical) = 76
Start time [ms] = 2250
End time [ms] = 2400

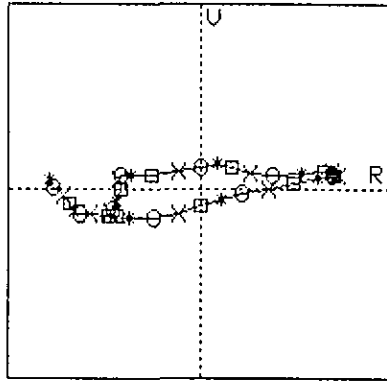
Sample interval [ms] = 2 * - O - X - □

8. Hodograms of random noise.

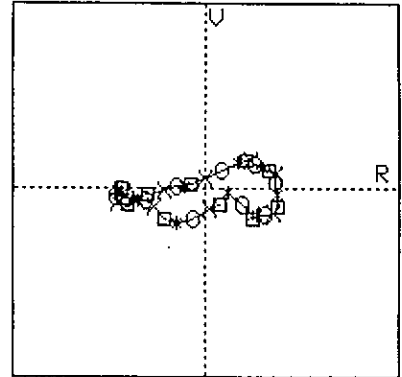
RECORD 16



Trace # (Radial) = 5
 Trace # (Vertical) = 6
 Start time [ms] = 1790
 End time [ms] = 1870



Trace # (Radial) = 7
 Trace # (Vertical) = 8
 Start time [ms] = 1790
 End time [ms] = 1870

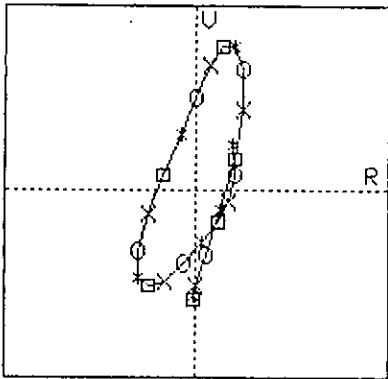


Trace # (Radial) = 13
 Trace # (Vertical) = 14
 Start time [ms] = 1790
 End time [ms] = 1870

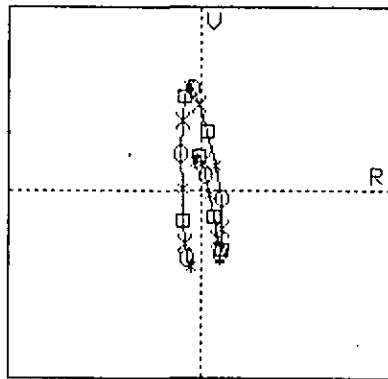
Sample interval [ms] = 2 * - O - X - □

9. Hodograms of P-SV reflection at 1800 ms.

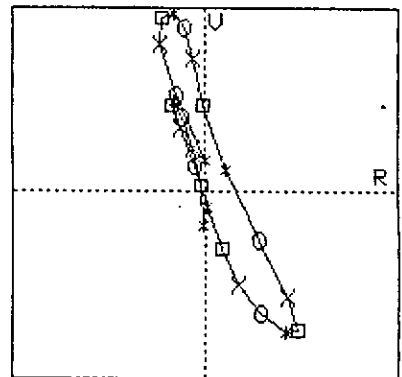
RECORD 16



Trace # (Radial) = 7
 Trace # (Vertical) = 8
 Start time [ms] = 500
 End time [ms] = 550



Trace # (Radial) = 9
 Trace # (Vertical) = 10
 Start time [ms] = 500
 End time [ms] = 550



Trace # (Radial) = 11
 Trace # (Vertical) = 12
 Start time [ms] = 500
 End time [ms] = 550

Sample interval [ms] = 2 * - O - X - □

10. Hodograms of P-SV reflection at 550 ms.

those on the radial channel. The rotation of the hodogram across the three traces shows the phase delays between the P- and SV-waves.

Basement occurs at about 2100 ms. in two-way P-P traveltime and is a strong reflector which can be observed on both vertical records 16 (Figure 1b) and 65 (Figure 3b). Hodograms run on the same reflection for each of the records produce dramatically different results. Figure 11 is the hodogram set for three adjacent traces on record 65. Although there is some radial excursion on trace 7 (labelled 13 and 14), the particle motion is primarily vertical, as expected. However, when the hodograms are computed over the same window on record 16, the particle motion appears completely random (Figure 12). There is as much or more radial motion as vertical, showing that analysis of the vector wave field cannot easily be performed if either component is excessively noisy. The geophones separated the components quite well so that a strong, clean reflection is visible on the vertical channel (Figure 1b), even though the hodogram indicates strong radial contamination.

Dynamic Range

Besides bandwidth and wave propagation, one of the primary attributes of noise which we must determine is its amplitude relative to signal. The range of amplitudes which can be recorded is limited by the recording equipment and the A/D resolution. Careful examination of the actual amplitudes of signal and noise is necessary in order to determine the dynamic range of the system needed to record the signal with full fidelity.

A comparison of various noise levels is shown in Figure 13. Absolute amplitudes are plotted on a logarithmic scale and represent millivolts $\times 10^5$. The scales in each figure are the same to allow comparison. Amplitudes were picked off the raw data for shot 16 across one noise window (ie. no visible reflection energy) from 1250 to 1650 ms. and a later noise window from 2800 to 3200 ms. for all 48 traces and for both channels. Because the time windows are constant, plots of these data show how the general noise level varies with offset.

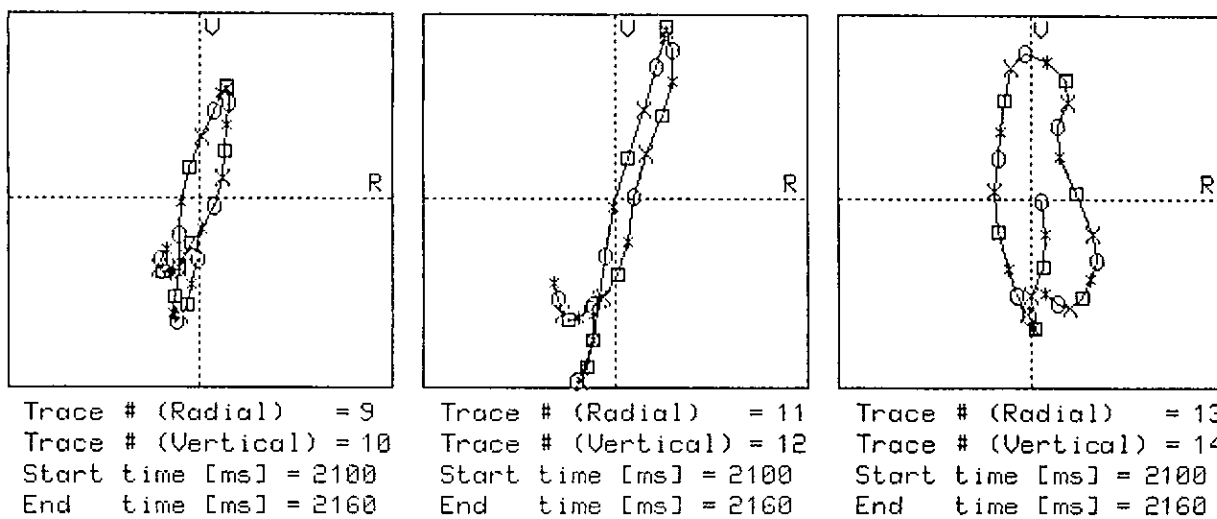
The results from the vertical channel are plotted in Figure 13a along with the P-P reflection signal. The reflection was picked on the outer 25 traces but then was masked by noise. At the longer offsets, signal levels are slightly higher than general noise levels, but noise levels increase rapidly near the shot, particularly for the earlier time window. Both noise windows occur after the reflection arrival.

Amplitudes for the same time windows and the P-SV signal are plotted in Figure 13b. Noise levels in both windows are very similar to the vertical channel. The first noise window, R1, occurs before the reflection and is slightly higher in amplitude. The second window, R2, is after the reflection and has slightly lower amplitude. Significantly, the amplitudes of the P-P and P-SV reflections are roughly equivalent, ranging from about 8×10^5 to 3×10^6 . Both components have an average amplitude of about 1×10^6 on the traces represented in these plots.

The signal amplitudes at near offsets could not be picked off the shot records and so were estimated from synthetic data. Figure 14 shows synthetic shot gathers based on the geology of this area and using the Field School spread geometry. P-P reflections have similar amplitudes to P-SV reflections for about the outer half of the gather. As offset decreases, P-P reflections increase in amplitude and P-SV reflections diminish.

The amplitudes of the linear, coherent noise are plotted in Figure 13c. P- and S-headwave energy on the near-offset trace was clipped by the recording instruments at 2×10^9 , 70 dB higher than the reflection amplitudes in Figures 13a and 13b. The Rayleigh wave on the radial channel has an amplitude of 1×10^9 at the nearest offset and closely

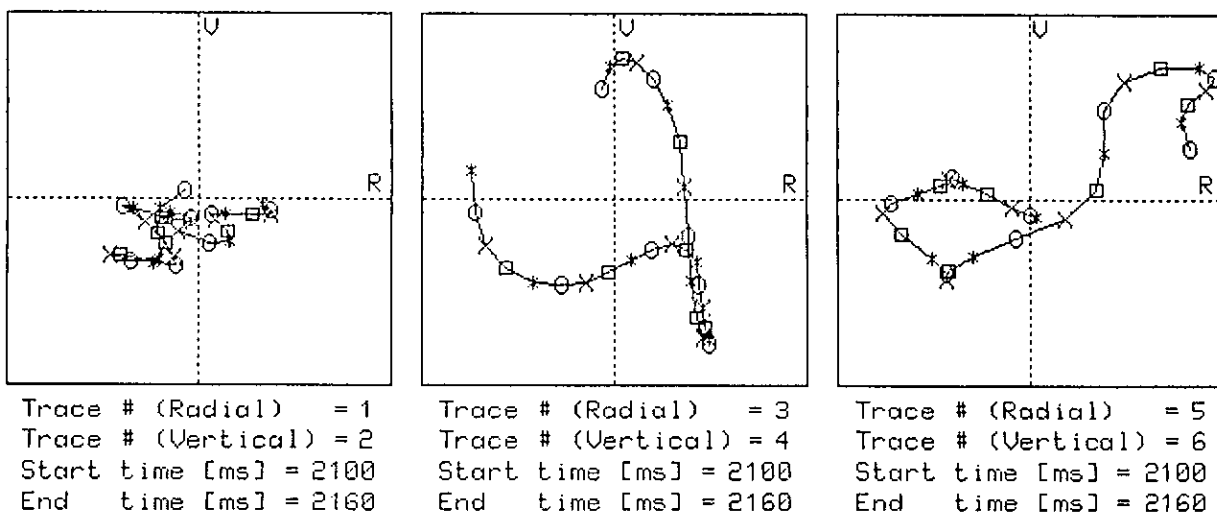
RECORD 65



Sample interval [ms] = 2 *—○—×—□

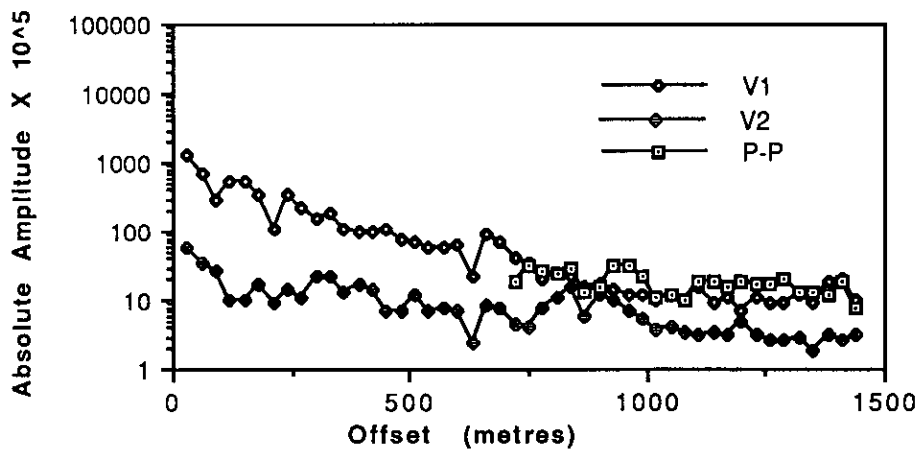
11. Hodograms of P-P basement reflection, record 65.

RECORD 16

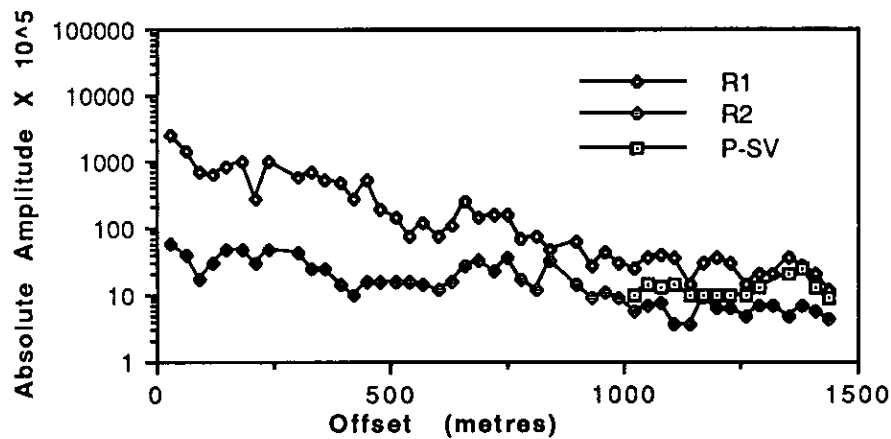


Sample interval [ms] = 2 *—○—×—□

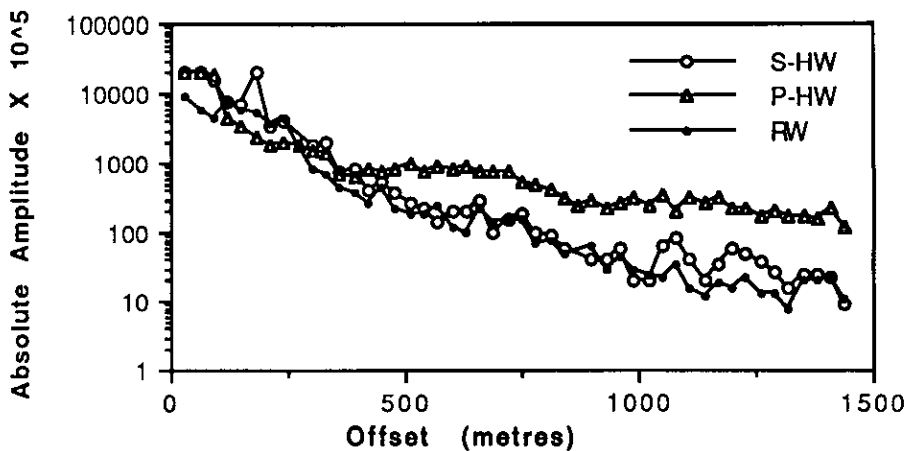
12. Hodograms of P-P basement reflection, record 16.



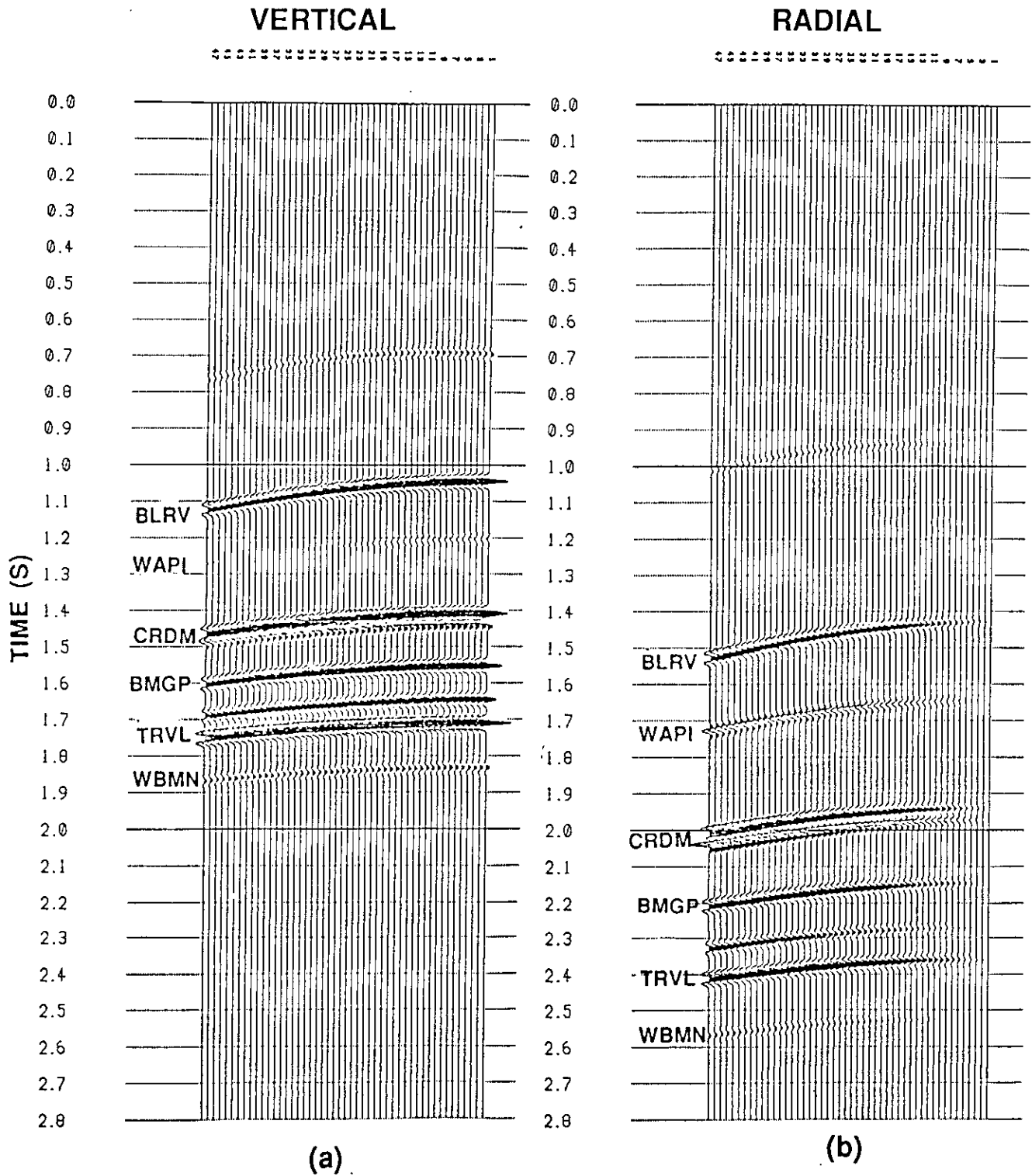
13a. Amplitude vs. offset from vertical channel of record 16 for: P-P reflection at 1050 ms., noise window from 1250 to 1650 ms. (V1), noise window from 2800 to 3200 ms. (V2).



13b. Amplitude vs. offset from radial channel of record 16 for: P-SV reflection at 1850 ms., noise window from 1250 to 1650 ms. (R1), noise window from 2800 to 3200 ms. (R2).



13c. Amplitude vs. offset from vertical channel of record 16 for: P-headwave (P-HW) and Rayleigh wave (RW); and from radial channel of record 16 for S-headwave (S-HW).



14. Synthetic shot gathers using Field School geometry:
a) P-P reflections; b) P-SV reflections.

from Lawton and Harrison, 1990, this volume.

tracks the S-headwave curve as offset increases. At far offsets, S-headwaves and Rayleigh waves are approaching signal amplitude and P-headwaves exceed signal by about 20 dB.

On all the curves, random trace to trace amplitude variations are evident. With single-point receivers, variations in geophone coupling are not averaged out as they are with arrays. Poor geophone plants show up as sudden drops in amplitude at traces 28 and 42.

DISCUSSION

The factors which must be considered when acquiring multicomponent data compel us to take another look at noise. The insights gained from a careful examination of the nature of both signal and noise on multicomponent data also has important implications for how we acquire and process conventional seismic data.

Shots 16 and 65 displayed quite different noise characteristics. Surface-wave energy was the dominant noise pattern on record 16, which had a near offset of 30 metres. Record 65 had a far enough offset to be beyond the high-amplitude ground roll, but the signal was obscured by reverberating refraction energy. Windy conditions induced the high-frequency noise evident on the records for shot 65.

Analysis of record 16 showed that headwaves had similar frequency content to signal in the P-wave case and higher frequency than signal in the SV-wave case. Substantial P-headwave energy was evident on the radial channel and interfered with a shallow P-SV reflection which arrived before the S-headwave.

Hodograms demonstrated that Rayleigh-wave energy was 2 to 3 times greater on the radial channel than on the vertical because of the elliptical nature of the particle motion. Thus, although the SV-wave had the same amplitude as the P-wave, the noise level on the radial channel was higher. Amplitude analysis revealed that SV-wave signal bandwidth overlapped with that of the surface-wave energy. Low-cut filtering, conventionally used for P-wave data, would be difficult to apply to the radial channel. Filtering which effectively reduced ground roll would also attenuate signal.

Low-frequency random noise was also significant on the near-offset records. Although this tended to stack out in processing, its prominence on the field records made it difficult to access the data quality during acquisition. This type of noise problem was largely the result of single-point receivers and was considerably reduced by geophone arrays, which tended to average out random shot noise. Geophone arrays were also effective at attenuating long-wavelength coherent noise, such as surface waves.

Particle motion analysis through the use of hodograms demonstrated that component separation of the geophones was quite good. Noise on one channel did not appear to affect the reflection energy on the orthogonal channel. This was shown for a P-SV reflection arriving at the same time as a P-headwave and also for a P-wave reflection arriving with low-frequency radial noise. Although the reflection signal was recovered in both cases, noise contamination from orthogonal channels could impede vector analysis of the wave field.

Measurements from record 16 indicate that P-P and P-SV reflection amplitudes are roughly equivalent at offsets from 1000 to 1500 metres. At this offset, both coherent and random shot-generated noise have decreased to about the same amplitude level as signal. Using synthetic data to extrapolate reflection amplitudes to near offset, P-P signal should still be recoverable from the deeper section. For shallow events at near offsets the instrumentation may be unable to adequately resolve the signal, due to high noise amplitudes forcing a reduction in gain. This assumes an A/D resolution of 78 dB. Amplitude increases in P-wave reflection signal near the shot are insufficient to offset the increase in noise amplitude, which rises by three orders of magnitude (60 dB). Because the P-SV signal decreases in amplitude at low offsets, the amplitude range between noise

and signal exceeds the A/D resolution and the signal is unrecoverable. On record 16, loss of P-SV signal resolution was estimated to occur at about 300 metres offset.

Trace to trace amplitudes variations on the multicomponent records were attributed to the quality of individual geophone plants.

CONCLUSIONS

1. The bandwidth of surface-wave energy and other low-frequency shot noise was separated from the P-P signal bandwidth but overlapped with that of the P-SV signal. Central frequencies were about 10 Hz for surface waves, 15 Hz for P-SV waves, and 30 Hz for P-P waves.
2. Coherent surface-wave energy was identified as a Rayleigh wave with retrograde elliptical motion. The amplitude was 2 to 3 times greater in the radial direction than in the vertical direction. At near offsets, Rayleigh-wave amplitude on the radial channel was at least 3 orders of magnitude (60 dB) greater than the signal amplitude, but decreased to the same level as the signal at an offset of about 1000 metres.
3. Refraction energy had a central frequency of about 35 Hz for both P-waves and S-waves. Headwave energy was the highest amplitude noise on the records, exceeding the predicted signal amplitude by at least 3 orders of magnitude at near offsets.
4. The geophones were effective at separating radial and vertical channels even when hodograms indicated that high-amplitude noise had arrived simultaneously on the orthogonal channel.
5. The amplitudes of the P-P waves and the P-SV waves were roughly equivalent across offsets from 1000 to 1500 metres. Poorer S/N ratios on the radial records were attributed to other factors, such as greater surface-wave contamination. .
6. At near offsets, the amplitude range between converted-wave signal and shot-generated noise exceeded the A/D resolution of the instrumentation, resulting in loss of signal.
7. The vertical records, with a single-point receiver, had more surface-wave and other shot-generated noise contamination than equivalent shot records from the conventional survey, which used geophone arrays. After bandpass filtering, record quality was comparable. Single-point receivers also resulted in trace to trace amplitude variations which were attributed to differences in geophone coupling from station to station.

ACKNOWLEDGEMENTS

This research was supported by the CREWES project and the Department of Geology and Geophysics at the University of Calgary.

REFERENCE

- Sheriff, R.E., 1984, Encyclopedic Dictionary of Exploration Geophysics, 2nd ed.: Society of Exploration Geophysicists, 114, 198.